Hindawi
Mathematical Problems in Engineering
Volume 2019, Article ID 2545347, 15 pages
https://doi.org/10.1155/2019/2545347

Research Article

Computational Study of Gas-Solid Flow in a Horizontal Stepped Pipeline

Zhengquan Li,[1,2] **Kaiwei Chu**,[3] **Renhu Pan**,[4] **Aibing Yu**,[2,4] **and Jiaqi Yang**[1]

[1]*International Research Institute for Minerals, Metallurgy and Materials, Jiangxi University of Science & Technology, Ganzhou 341000, China*
[2]*Laboratory for Simulation and Modelling of Particulate Systems, Chemical Engineering, Monash University, Clayton, Melbourne, VIC 3800, Australia*
[3]*School of Qilu Transportation, Shandong University, Jinan 250002, China*
[4]*Fujian Longking Corporation, Longyan 364000, China*

Correspondence should be addressed to Zhengquan Li; qqzhengquan@163.com and Kaiwei Chu; k.chu@sdu.edu.cn

Received 5 June 2019; Accepted 19 July 2019; Published 15 September 2019

Academic Editor: Dongmin Yang

In this paper, the mechanism governing the particle-fluid flow characters in the stepped pipeline is studied by the combined discrete element method (DEM) and computational fluid dynamics (CFD) model (CFD-DEM) and the two fluid model (TFM). The mechanisms governing the gas-solid flow in the horizontal stepped pipeline are investigated in terms of solid and gas velocity distributions, pressure drop, process performance, the gas-solid interaction forces, solid-solid interaction forces, and the solid-wall interaction forces. The two models successfully capture the key flow features in the stepped pipeline, such as the decrease of gas velocity, solid velocity, and pressure drop, during and after the passage of gas-solid flow through the stepped section. What is more important, the reason of the appearance of large size solid dune and pressure surge phenomena suffered in the stepped pipeline is investigated macroscopically and microscopically. The section in which the blockage problem most likely occurs in the stepped pipeline is confirmed. The pipe wall wearing problem, which is one of the most common and critical problems in pneumatic conveying system, is analysed and investigated in terms of interaction forces. It is shown that the most serious pipe wall wearing problem happened in the section which is just behind the stepped part.

1. Introduction

In industries, there are always increasing needs to convey large quantities of bulk solids over a long distance (up to 1-2 km). In such cases, the long-distance high-pressure dense-phase pneumatic conveying systems are usually employed. This system mainly consists of storage pumps, conveying pipelines, and cyclone separators. In such a system, the stepped pipeline rather than conventional pipeline is usually used. This is because that, in the conventional pipeline and high-pressure conditions, the gas and solid velocities will be too high at the end of the pipeline due to the compressibility of the gas. High velocity can cause solids attrition, pipe wear, and a large pressure loss. A large pressure loss also means that more power is needed for the transportation. Therefore, keeping the conveying air velocity as low as possible is very important. The stepped pipeline (Figure 1) provides a solution for this problem.

Although the advantages of using stepped pipelines are considerable compared to single-bore pipelines, the use of stepped pipelines in high-pressure systems has been a long and slow development. Part of this was probably due to the lack of understanding of the mechanisms governing the gas-solid flow characters in the stepped pipeline. There was very little published information on the subject, and only a few universities, on a worldwide basis were undertaking research in the area [2]. In the last decade, more and more researchers paid attention to this area, but published information is still limited.

Generally, studies on gas-solid flows in the stepped pipelines have employed two methods of investigation: experimental and numerical simulation methods [3].

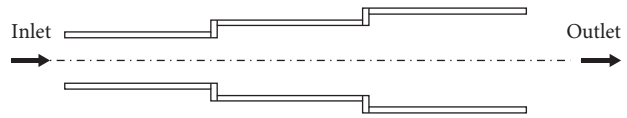

Figure 1: Sketch of stepped pipeline [1].

In the experimental investigation category, Tashiro et al. [4–7] studied the sudden expansion of a gas-solid two-phase flow in a pipe when the flow direction was vertically downward and upward, in addition to investigating the influence of the diameter ratio of a sudden expansion circular pipe in the case of a gas-solid two-phase flow. Further, velocities of solid particles and gas phase when flowing through a sudden expansion in the vertical stepped pipeline have also been measured by several authors [8–10]. Solid particles have been found to move faster than the carrier fluid almost everywhere in the expanded flow region, and conversely, small particles (i.e., submicron particles) are captured by the recirculating flow, from which the large particles with a high inertia could escape. Founti and Klipfel [11] investigated the effects of particle-to-particle collisions on the characteristics of the particle motion in a vertically downward flow through a sudden expansion, both experimentally and computationally. Experiments and predictions demonstrated that, for semi-dense sudden expansion flows, particle dispersion is mainly controlled by the relative magnitude of the time elapsed between successive collisions, the local value of the particle relaxation time, and the eddy time scale. The details of laminar axisymmetric sudden expansion flows such as the distance to the reattachment, redevelopment length, and strength of the recirculating flow have also been widely investigated through a flow visualization technique [12, 13] and particle image velocimetry (PIV) measurements [14]. These results are useful in solving some practical problems. However, the flow direction in most of these researches is vertically downward and upward. The microcosmic mechanisms underlying the gas-solid flow in a horizontal stepped pipeline are still not clearly understood. In principle, computer modelling and simulations can overcome this problem.

In the numerical simulation investigation category, Gundogdu et al. [15] analysed the pressure loss through a sudden expansion in two-phase pneumatic conveying lines and developed a new model called the slip flow model, which takes into account the slip velocity between gas and solid phases, evaluated by coupling the well-known separated flow model with the empirical slip ratio predictions in the literature. Bae and Kim [16, 17] studied the pressure losses in turbulent flows through axisymmetric sudden expansions and the effect of Reynolds number with the two fluid model (TFM). The obtained results showed that for the cases where the jet remains attached to the chamfer surface, the reattachment length, separation point, and irreversible pressure drop occurring from the sudden expansions are less sensitive to the Reynolds number. A great progress has been made in the understanding of the mechanism governing the complex gas-solid flow in stepped pipelines by using the numerical approach, and what should be pointed out is that almost all the numerical studies have been based on the TFM. TFM is preferred in process modelling and applied research because of its computational convenience. However, as pointed out by Zhu et al. [18, 19], the TFM approach is unable to model the discrete flow characteristics of particles of different properties. Without the particle scale information about the mechanisms governing the gas-solid flow, the design, optimization, and scale-up of the stepped pipeline and its further application will be hindered. Luckily, the discrete flow characteristics of particles can be studied by the combined discrete element method (DEM) and computational fluid dynamics (CFD) model (CFD-DEM) [20, 21].

CFD-DEM model can obtain particle scale information which is useful for fundamental understanding while TFM can model industrial scale system [22, 23] where billions of particles are encountered. Some cases studied by the TFM are hard to be modelled by the CFD-DEM model due to limited computational resource. To maximize the advantage of TFM and CFD-DEM, both will be used to study the gas-solid flow in a horizontal stepped pipeline. The TFM will be used in this paper to investigate the mechanisms governing the gas-solid flow in relatively macroscopic view, in terms of solid and gas velocity distributions, pressure drop, and process performance. The flow characteristics in the stepped pipeline in the particle scale will be studied by using the CFD-DEM method. Meanwhile, the reason of large size solid dune and pressure surge phenomena suffered in the stepped pipeline will be investigated macroscopically by TFM and microscopically by CFD-DEM. The section in which the blockage problem most likely occurs in the pipeline will be confirmed. The pipe wall wearing problem, which is one of the most common and critical problems in pneumatic conveying system, will be analysed in terms of interaction forces.

2. Mathematical Model

The TFM [18, 24–28] and CFD-DEM [18, 29–36] used for the present work has been well documented in the literature. For brevity, only a brief description of these two methods is given here.

Both the solid and gas phases are treated as continuum phases in TFM. There are two sets of governing equations in TFM: one is called Model A and the other Model B [25]. The major difference between Model A and Model B is that Model A assumes that gas and solid phases share the pressure while Model B assumes that pressure only acts on gas phase. Both the Model A and Model B can give similar results [18, 27]. In this work, Model B is used. Thus, the conservations of mass and momentum in terms of the local mean variables over a computational cell are given by

$$\frac{\partial \varepsilon}{\partial t} + \nabla \cdot (\varepsilon \mathbf{u}) = 0,$$
$$\frac{\partial (\rho_f \varepsilon \mathbf{u})}{\partial t} + \nabla \cdot (\rho_f \varepsilon \mathbf{u}\mathbf{u}) = -\nabla \mathbf{p} - \mathbf{F}_{pf} + \nabla \cdot (\varepsilon \boldsymbol{\tau}) + \rho_f \varepsilon \mathbf{g}, \quad (1)$$

where ε, $\mathbf{u}$, and t are, respectively, porosity, fluid velocity, and time; ρ_f, P, $\mathbf{F}_{pf}$, $\boldsymbol{\tau}$, and $\mathbf{g}$ are the fluid density and pressure, volumetric particle-fluid interaction force ($\mathbf{F}_{fp} = \sum_{i=1}^{k_c} \mathbf{f}_{pf,i}$, where k_c is the number of particles in a CFD cell), fluid viscous stress tensor, and gravity acceleration, respectively.

The frictional force is one of the most important forces on a particle by its surrounding fluid. The model formulation for the frictional force in TFM is

$$F_{\mathrm{f}} = \mu F_{\mathrm{N}}, \tag{2}$$

where F_{f} is the force of friction exerted by each surface on the other; μ is the coefficient of friction, which is an empirical property of the contacting materials; and F_{N} is the normal force exerted by each surface on the other, directed perpendicular to the surface.

For the CFD-DEM, the solid phase is treated as a discrete phase and described by the so-called discrete element method [34]. According to the model, the translational and rotational motions of a particle at any time, t, can be described by Newton's law of motion:

$$\begin{aligned} m_i \frac{d\mathbf{v}_i}{dt} &= \mathbf{f}_{\mathrm{pf},i} + \sum_{j=1}^{k_i} \left(\mathbf{f}_{\mathrm{c},ij} + \mathbf{f}_{\mathrm{d},ij}\right) + m_i \mathbf{g}, \\ I_i \frac{d\boldsymbol{\omega}_i}{dt} &= \sum_{j=1}^{k_i} \left(\mathbf{T}_{ij} + \mathbf{M}_{ij}\right), \end{aligned} \tag{3}$$

where m_i, I_i, and $\mathbf{V}_i$ and $\boldsymbol{\omega}_i$ are, the mass, moment of inertia, and translational and rotational velocities of particle i, respectively. The forces acting on particle i are the gas-solid interaction force, $\mathbf{f}_{\mathrm{pf},i}$, interparticle forces between particles i and j, which include the contact forces, $\mathbf{f}_{\mathrm{c},ij}$, and viscous damping forces, $\mathbf{f}_{\mathrm{d},ij}$, and the gravitational force, $m_i\mathbf{g}$. In this model, the gas-solid interaction force includes viscous drag force ($\mathbf{f}_{\mathrm{d},i}$) and pressure gradient force ($\mathbf{f}_{\mathrm{pg},i}$). The interparticle forces are summed over the k_i particles in contact with particle i. Torques, $\mathbf{T}_{ij}$, are generated by tangential forces and cause particle i to rotate, because the interparticle forces act at the contact point between particles i and j not at the particle centre. $\mathbf{M}_{ij}$ is the rolling friction torque that opposes the rotation of the i^{th} particle. The governing equations of gas phase are the same as those used in TFM [25].

The TFM used in this paper is based on the commercial ANSYS software and the CFD-DEM method used is based on the in-house codes developed by "SIMPAS" group at the Monash University. To take the advantages of the CFD developments already available, we have extended our CFD-DEM code with the commercial software Fluent as the platform, achieved by incorporating a DEM code into Fluent through its User Defined Functions (UDF). The computational domain for particle and fluid phases is the same, with the boundary meshes automatically generated in Fluent for the considered systems. The coupling of DEM and CFD at different time and length scales is achieved using the same scheme as that in our previous studies [33, 37–40].

3. Simulation Conditions

The stepped pipe investigated in this paper is sketched in Figure 2(a). The first half part of this pipeline is a conventional pipeline of 324 mm diameter, the second half part of it is a conventional pipeline of 400 mm diameter, and the total lengths of it is 34 m. There is a gradual expansion part between the two conventional pipeline parts. Figure 2(b) shows a part of the computational domain for the stepped pipeline; note that the whole computational domain of the stepped pipeline contains 83,000 structured CFD grids. In the TFM and CFD-DEM modelling, not periodic boundary, inlet and outlet is used to make the simulation conditions closer to real situation. All the simulations in this study are 2D. The other material properties and operational variables are shown in Table 1. As stepped pipelines are usually used at a high pressure, the density of gas phase used here is 2.45 kg/m^3.

To illustrate the improvement in the stepped pipeline, two single bore pipelines are also studied for the comparison purpose. The first conventional single pipeline has a 324 mm pipe diameter, which is the same as the first half part of the stepped pipeline. The second conventional single pipeline has a 400 mm pipe diameter, which is the same as the second half part of the stepped pipeline. Just one conventional single pipeline is sketched here for brevity (Figures 2(c) and 2(d)). The computational domains of the conventional pipelines of 324 mm and 400 mm diameters contain 28000 and 34600 structured CFD grids, respectively.

4. Results and Discussion

4.1. Working Mechanism of the Bypass System

4.1.1. Pressure Drop. For a given pipeline system, the pressure drop with gas only flow can provide a useful reference. For example, during the industrial application, if the pressure drop with gas only flow is higher than the referenced value, it may reflect that some conveying materials are still left in the pipeline, a material build-up on the pipeline walls, or even a partial blockage in the pipeline. Up to now, investigations on the empty stepped pipeline pressure drop has not been reported. In this study, the pressure drop is defined as the pressure difference between the inlet and outlet of the conveying pipeline. The empty stepped pipeline pressure drop will be studied firstly. For comparison purpose, the pressure drop results of empty single pipelines will also be considered, and the results are shown in Figure 3.

It can be seen very clearly that with an increase in air mass flow rate, the empty-line pressure drop in the single pipe goes up exponentially. Similar simulation results are obtained for the stepped pipes, but the increase is gentler. What is more, the stepped pipe has the smallest empty-line pressure drop. The empty-line pressure drop value of the stepped pipe is only about half of the 324 mm single pipe. Although the second half part of the stepped pipe has the same diameter with the other single pipe, 400 mm, the pressure drop value is still smaller than that of the single pipe. Besides, the results also indicate that the 400 mm diameter single pipe has a lower pressure drop than that of the 324 mm diameter single pipe. The empty-line pressure drop goes down with the increase of single pipe diameter for gas only flow.

For a fixed solid flow rate and solid loading ratio, many reported researches show that the stepped pipe can reduce the pressure drop by a large amount compared to a conventional single pipeline [1, 41]. In this study, the solid mass flow rate is 88 kg/s while the air mass flow rate is 1.5 kg/s.

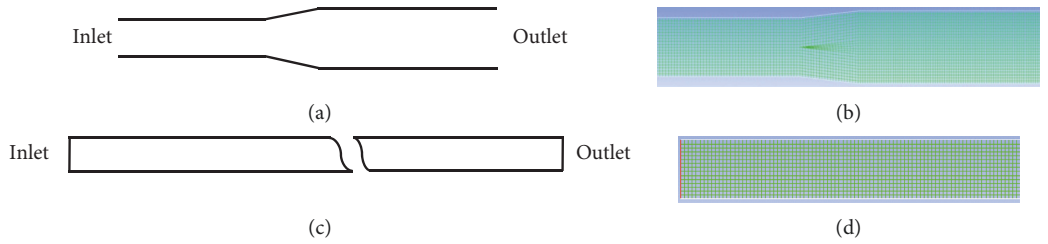

Figure 2: (a) A sketch of stepped pipeline, (b) structured CFD grids of the computational domain, (c) single pipeline, and (d) computational domain grid of single pipeline.

Table 1: Simulation parameters used in this work.

Numerical model	Parameters	Symbol	Units	Value
CFD-DEM	Solid mass flow rate		kg/s	0.89
	Solid density	ρ	kg/m^3	800
	Solid particle radius	R_i	mm	3
	Time step for solids	Δt	s	1×10^{-6}
	Solid velocities	v_p	m/s	6.4–24
	Gas density	ρ	kg/m^3	2.45
	Gas velocities	v_g	m/s	8–30
	Time step for gas	Δt	s	6×10^{-3}
TFM	Solid particle diameter	R_i	mm	0.8
	Solid density	ρ	kg/m^3	1400
	Solid velocities	v_p	m/s	3.2–20
	Inlet gas velocities	v_g	m/s	4–25
	Gas density	ρ	kg/m^3	2.45
	Time step	Δt	s	1×10^{-4}

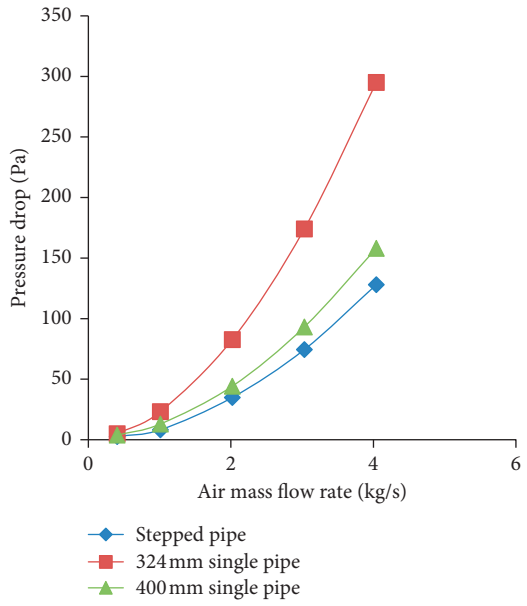

Figure 3: Relationship between empty-line pressure drop and air mass flow rate for TFM method.

Keeping the same solids and air mass flow rates, the gas-solid flows in the stepped pipe and conventional single bore pipes with 324 mm and 400 mm diameters are investigated. The distribution of static pressure near the stepped section can be seen from the numerical simulation results (Figure 4). The variations of the pressure drop in the stepped and single pipes can be seen in Figure 5.

It can be seen from Figure 4 that the static pressure changes more significantly in both sides of the stepped section than that in the stepped part itself. In addition, the first part of the stepped pipe has a more significant pressure drop change than that in the second part. These results indicate that the pressure drop is largely reduced when the gas-solid flow passes through the stepped section.

A characteristic feature of Figure 5 is that the fluctuations of the pressure drop are high, which are due to the appearance of the solid dunes that will be studied later on in other sections. This figure also shows that the pressure drops are 830 Pa, 1300 Pa, and 1050 Pa, for the stepped pipe, single pipe with 324 mm diameter, and the single pipe with 400 mm diameter, respectively. The stepped pipe has the lowest pressure drop compared to the other two conventional single pipes for the same mass flow rate and solid loading ratio, which agrees well with the experimental results of Mills [1].

For investigating relationship between the pressure drop and air mass flow rate, the solid mass flow rate is kept at 88 kg/s. The single pipe of 400 mm diameter is studied to compare with the stepped pipeline. The simulation results are shown in Figure 6.

It can be seen that the pressure drop goes up with the increase of air mass flow rate in the case of the stepped pipe. A lower pressure drop can be found in the case of the stepped pipeline compared with that of the 400 mm diameter single pipeline. The results also indicate that the pressure drop difference between the stepped pipe and single pipe becomes larger with an increase in the air mass flow rate.

In addition, a lower pressure drop means lower energy consumption. The above results show that higher flow rates can be achieved with a lower pressure drop, resulting in less energy consumption for a given gas-solid flow in the stepped pipeline than that in the conventional single pipeline. The improvement of the performance is huge when the stepped pipeline is used, which agrees well with the theoretical analysis results [1].

To study the effects of different pipe sizes on the pressure drop, three cases were studied. The first halves of the stepped pipelines are conventional pipelines of 243 mm, 283.5 mm, and 324 mm, and their second halves are conventional pipelines of 300 mm, 350 mm, and 400 mm diameters,

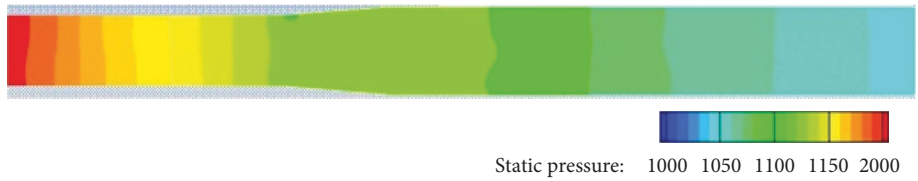

Figure 4: Distribution of static pressure near the stepped section with TFM.

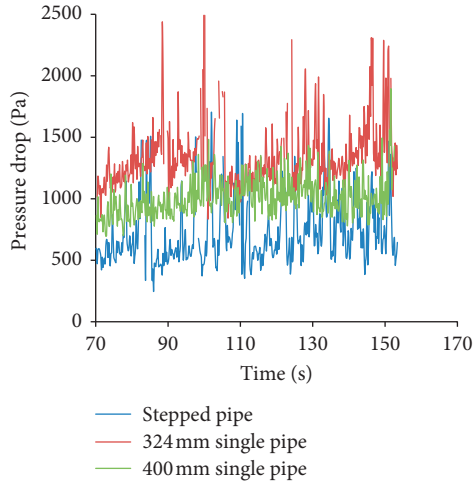

Figure 5: Variation of the pressure drop in the stepped pipe and conventional single pipe for a fixed solid mass flow rate of 88 kg/s and fixed loading ratio with TFM.

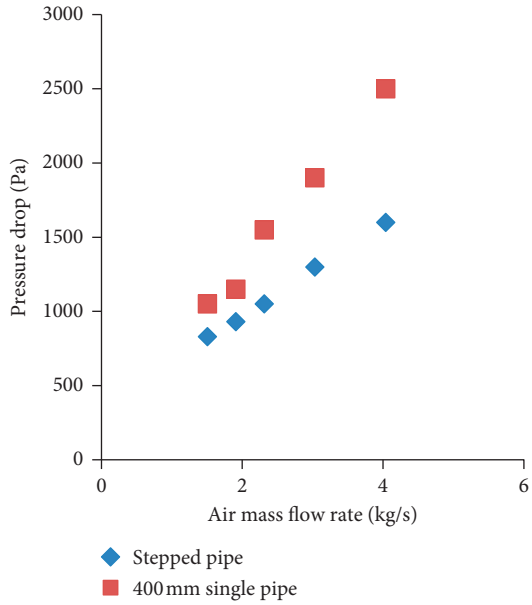

Figure 6: Relationship between pressure drop and air mass flow rate with TFM method and a fixed solid mass flow rate.

respectively. The operational conditions are that they all have the same solid mass flow rate of 88 kg/s, and a fixed solid loading ratio. The simulation results are shown in Figure 7.

It can be seen from Figure 7 that the pressure drop reduces with an increase in stepped pipeline diameter. These

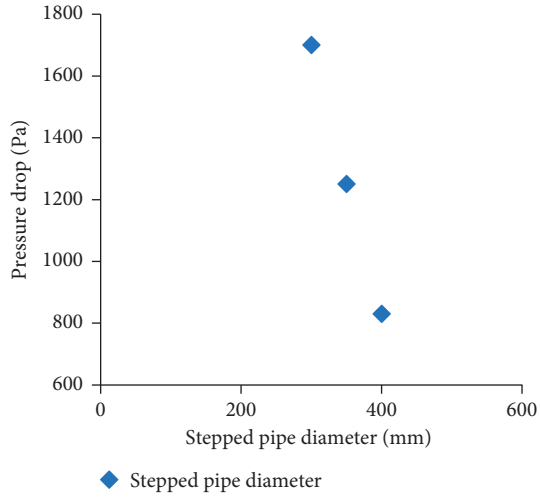

Figure 7: Relationship between stepped pipeline diameters and pressure drop with TFM.

results also indicate that the energy consumption decreases with increasing of pipe diameter for the stepped pipeline.

4.1.2. Gas Velocity. For the study of gas velocity, cases of gas only flow in the stepped and other two single pipes of 324 mm and 400 mm diameters are studied firstly. The air mass flow rate is kept at 2 kg/s in each case. From Figures 8(b)–8(d), it can be seen very clearly that the stepped pipe has the lowest exit velocity. For the conventional single pipe, the results of Figures 8(c) and 8(d) also indicate that the gas only exit velocity decrease with an increase in pipe diameter. For the stepped pipeline, Figure 8(a) reveals that there is a sudden decrease in gas velocity at the stepped part, which agrees well with Mills' theoretical analysis results [1]. This is because the gas density goes down sharply at this part with the enlargement of pipe diameter size.

The relationship between the air mass flow rate and exit gas velocity is also studied here (Figure 9). A linear relationship between the gas velocity and air mass flow rate can be seen from Figure 9 for the stepped pipeline and conventional single pipelines. The stepped pipe has a lower exit gas velocity compared to the single pipe under the same operational conditions. With the increase of air mass flow rate, the difference between the exit gas velocity of the stepped pipe and those of single pipes becomes larger. The exit gas velocity decreases with an increase in single pipe diameter.

For the gas-solid flow, the gas velocity is very important. If the gas velocity is too high, the particle conveying velocity

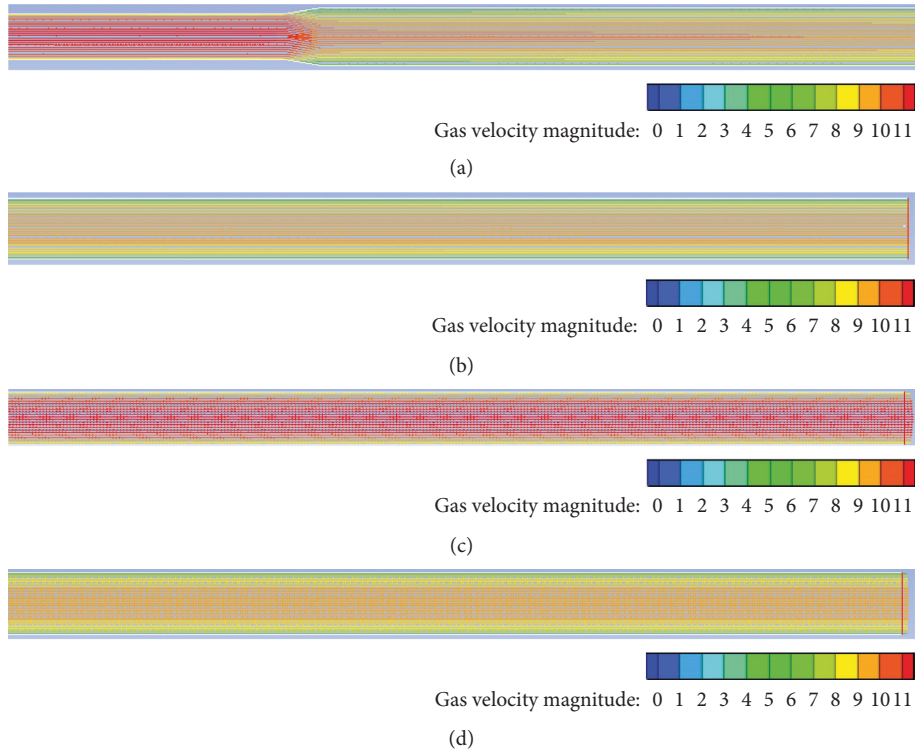

Figure 8: Gas velocity field in gas only flow with TFM, coloured by velocity magnitude (m/s) on the same scale: (a) velocity field at the stepped part of the stepped pipe; (b) velocity field near the exit of stepped pipe; (c) velocity field near the exit of 324 mm single pipe; (d) velocity field near the exit of 400 mm single pipe.

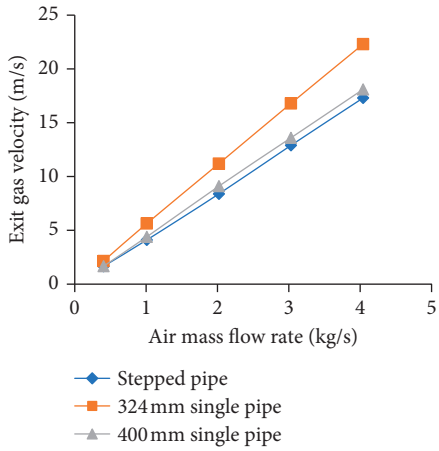

Figure 9: Relationship between exit gas velocity and air mass flow rate in gas only flow in the TFM numerical method.

will be high. A higher-speed material flow can cause an abrasive material to produce excessive and premature wear on the conveying line and other material-contact components. To study the gas velocity in the stepped pipe and single pipelines of 324 mm and 400 mm diameters, the solids mass flow rate is kept at 88 kg/s and solids loading ratio at 58.7. The numerical results are shown in Figure 10. It can be seen from the Figure 10 that the gas velocity in the single pipeline of 324 mm pipe diameter is biggest. When the pipe diameter of single pipeline is increased to 400 mm (see Figure 10(c)), a lower gas velocity can be found, but the gas velocity near exit is still higher than the exit gas velocity of the stepped pipe. The results also show how huge an improvement can be obtained by using a stepped pipe in the same situation. There is a sudden change in the gas velocity when the gas-solid flow passes through the stepped part of the stepped pipeline. The gas velocity after the stepped point is about only half of the gas velocity before this point.

4.1.3. Solid Velocity. For horizontal pneumatic conveying, the excessive wear and premature wear of the conveying line and other material-contact components, damage to friable material, the particle degradation, even blockages in the conveying pipeline, and so on are all directly or indirectly related to the velocity of solids. So, the study of solid velocity is very important.

The study of the solid velocity is also started from a comparison between the stepped pipeline and two conventional single pipelines. The identical operational conditions, namely, a solid mass flow rate of 88 kg/s and solid loading ratio of 58.7 are used for all three pipelines. The results are shown in Figure 11.

It can be seen from Figure 11 that the solid velocity is reduced largely when the gas-solid flow passes through the stepped section of stepped pipeline. The solid velocity is lower in the bottom part of all the pipes and is relatively higher in the upper part. Figure 11(b) shows that the solid velocity is higher over a longer section in the case of 324 mm diameter single pipeline than in the case of 400 mm diameter

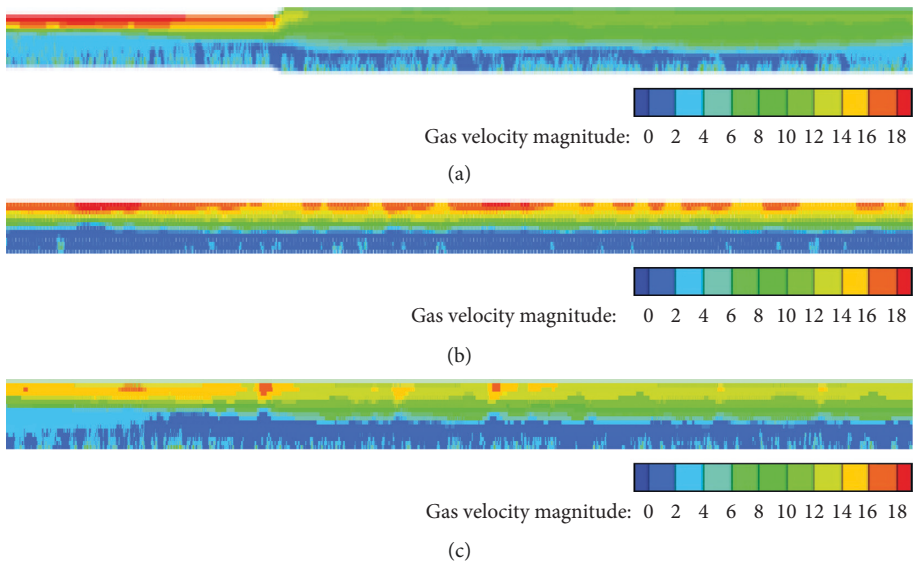

Figure 10: Gas velocity field in gas-solid flow with TFM, coloured by velocity magnitude (m/s) on the same scale, with air mass flow rate of 1.51 kg/s and solid mass flow rate of 88 kg/s: (a) stepped pipe; (b) 324 mm single pipe; (c) 400 mm single pipe.

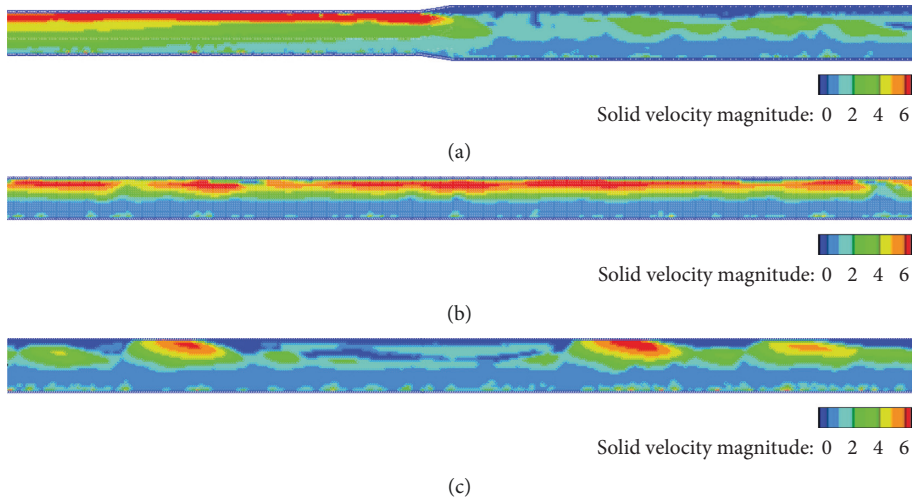

Figure 11: Solid velocity in gas-solid flow with TFM: (a) the stepped section of the stepped pipeline; (b) 324 mm diameter single pipeline; (c) 400 mm diameter single pipeline.

single pipeline (Figure 11(c)). It can be also inferred from the figures that the solid velocity decreases with the increase of pipeline diameter. In addition, the solid velocity in the second section of stepped pipeline is the lowest, compared to the solid velocity in the other two conventional single pipelines. This is one of the most important characteristics of pneumatic conveying with stepped pipeline systems, which is beneficial for the service cycle of conveying lines and the quality of the material conveyed.

4.1.4. Solid Dune/Pressure Surge Phenomena. The stepped pipeline often suffers the appearance of large size solid dune and pressure surge phenomena in engineering. Shown as Figure 11(a), the solid velocity in the upper part of first section of the stepped pipeline is very high, even the solid velocity in the bottom part of the first section is relatively high compared with conventional single pipelines. However, in the second section, there is a relatively thick layer of low-velocity solids, which will obviously hinder the high velocity gas-solid flow coming from the first section. In this case, a pressure surge or a potential blockage will happen in the conveying pipe. This situation will be investigated through the change of distribution of solids volume fraction in the stepped pipeline, shown as following.

Figure 12 shows the moving process of a solid dune formed through the stepped part of the stepped pipeline. The time interval between two consecutive snapshots is 0.2 s. It can be seen that the volume fraction of solids is high in the first part of stepped pipeline while it is low in the second part of the pipeline before the solid dune passes through the stepped section (Figure 12(a)). A solid dune is formed when

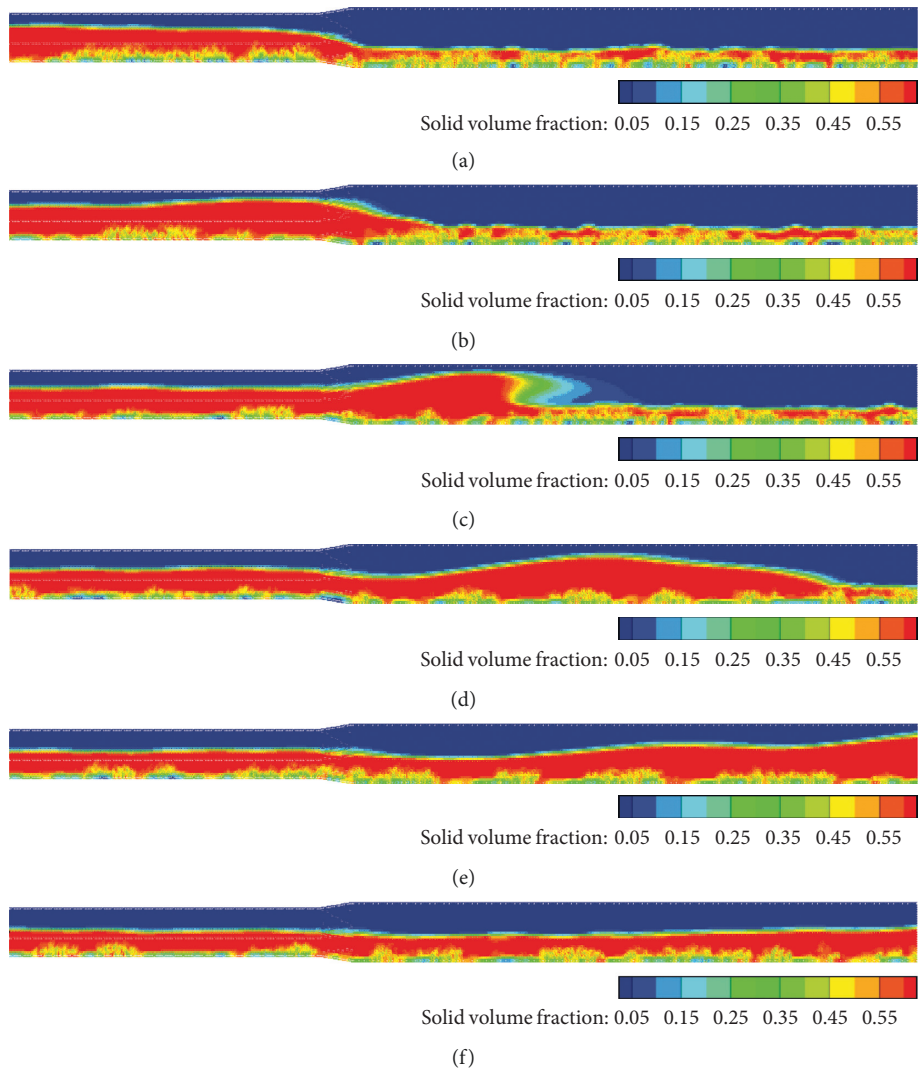

Figure 12: Distribution of solid volume fraction in the stepped pipeline when a solid dune forms and passes through the stepped section with TFM. (a) 5.2 s. (b) 5.4 s. (c) 5.6 s. (d) 5.8 s. (e) 6.0 s. (f) 6.2 s.

the flow of relatively high solid volume fraction in the first part meets with the flow of low solid volume fraction in the second part at the stepped section. This can be confirmed from a higher volume fraction at the entrance to the expanding section as can be seen from Figure 12(b). Further, it should be noted that the highest solid volume fraction does not appear in the stepped section, but rather it appears when the solid dune has just passed through the stepped section, as seen from Figure 12(c). After that, the solid dune collapses and disappears gradually; see Figures 12(d)–12(f). The solid volume fraction goes down gradually along the length of the second part of stepped pipe.

4.1.5. Mechanisms Governing Solid Dune/Pressure Surge Phenomena. The appearance of large-size solid dune increases the chance of potential blockage, and also causes the appearance of pressure surge due to the resistance from solid dune. A blockage is the most serious problem in the pneumatic conveying. The system will stop working if the blockage appears during the working process of conveying. The pressure surge is very harmful to the conveying system too. If the conveying system's pressure surges, the conveying tubes may be damaged due to excessive pressure, and the material conveyed may also be degraded due to the solids being subjected to acceleration or deceleration within a short period of time, as a result of the pressure surge. So, exploring the forming reason of the solid dune in particle scale is very necessary.

It can be seen from Figure 12 that the appearance of large size solid dune is mainly in the stepped section of the stepped pipeline. Understanding the mechanisms governing the gas-solid flow in the stepped section in particle scale is the first and foremost condition to tackle this problem. As stated in the introduction part, the TFM model is preferred in process modelling and applied research. The CFD-DEM method is more suitable for the study in particle scale. Therefore, the CFD-DEM method will be used in this section to study the gas-solid flow passing through the stepped part.

What should be pointed out here is that the CFD-DEM study will base on a scaled down version of the stepped pipe used above, for the purpose of reducing the computational burden. The first part of the scaled-down stepped pipe is a single pipeline of 45.6 mm diameter, and the second part is a single pipeline of 56.3 mm diameter pipe. The total length of the stepped pipe is 10 m. The material properties and other variables are the same as shown in Table 1.

Figure 13 shows the CFD-DEM results of the spatial solid velocity changing process when a solid dune passes through the stepped section. The time interval between consecutive snapshots is 0.03 s.

It can be seen clearly form Figure 13(a) that there is a high solid velocity layer in the upper part of first section of stepped pipeline, when a low solid velocity layer is in the bottom part of the first section. Further, it should be noted that the velocity of the "low-velocity" solids layer is still high compared to the solid velocity in the second part of the stepped pipeline. In Figure 13(b), when the solids layer of high velocity in the first part meets the solids layer of low velocity in the second part, the high velocity solids layer from the first part flows ahead through the space above the low-velocity solids layer in the second part. A solid dune is formed at this point. But this solid dune is not moving ahead as a whole at this time. When the dune moves along the second part of stepped pipe, the high velocity layer in the upper part of the dune continually picks up a relatively thick layer of solids of low velocity in front of it (Figure 13(c)) and a large solid dune is formed. After that, the picked-up solids layer of low velocity is accelerated by the high-velocity solids layer in the upper part of the dune, and the dune moves ahead seemingly as a "whole" (Figure 13(d)). But in fact, the upper part of the solid dune moves faster leaving the bottom part behind, and the solid dune "collapses" and disappears gradually (Figure 13(e)). These phenomena are similar to the observations reported in the experimental work of Wypych and Yi [42] and the simulation study by Kuang and Yu [43].

Figure 14 shows the distribution of time-averaged solids concentration and porosity when a dune passes through the stepped section.

Figure 14 indicates that a low solid concentration can be found in the stepped section, while a high solid concentration appears before and after the stepped section. Before the stepped section, the high solids concentration is in part due to the conveying pipe in this section being a single pipe, and the appearance of small dunes or clusters is a typical characteristic of the stratified flow regime; the hindering of the low-velocity solids layer in and after the stepped section also has an effect on this phenomenon. In the stepped section, the solids concentration is low and the porosity is high. The reason for the low solids concentration can be explained as follows: although the gas velocity is reduced largely in this section, due to the effects from the inertia and gravity, the solids can still flow ahead very smoothly. After the stepped section, a relatively high solids concentration can be found, and this is mainly due to the presence of thick layer of low-velocity solids in this section.

4.2. Forces Governing Particle Motion. The motion of solids is governed by the forces acting on it. Therefore, analysis of the collective interactions between solids, solids and walls, and solids and gas can help understand the underlying mechanisms. The interaction forces will be investigated in the following sections.

4.2.1. Gas-Solid Interaction Force. The gas-solid interaction force mainly includes the gas-solid drag force and pressure gradient force (PGF), and it is the main driving force in the gas-solid flow. Figure 15 shows the normalized total and averaged forces acting on solids from gas for different solid loading ratios. For convenience, the solid-solid force and solid-wall force are also included in the figure. It should be noted that the forces on a particle are all normalized dividing by the gravitational force of the particle.

It can be seen from Figure 15(a) that the total drag force decreases slightly and then increases gradually with solid loading ratio. This should be a result of comprehensive effect of gas velocity, solids concentration, and total number of solid particles. The total PGF increases with the solid loading ratio. The averaged drag force and PGF decrease with solid loading ratio. The increase of the total PGF should correspond to the total solid number increasing in the pipe with solid loading ratio (Figure 16). Figure 16 indicates that the total particle number increases linearly with the solid loading ratio. The decrease of the average drag force and PGF should be due to the decrease of the velocity in the flow direction and decrease of pressure drop in the stepped pipeline. The total and averaged drag forces are both larger than the PGF, which should mean that the drag force is more dominant for the gas-solid flow in the stepped pipe.

Figures 17 and 18 show the spatial distributions of gas-solid drag force and PGF near the stepped section. It can be seen that the directions of gas-solid drag force and PGF are all dominantly in the gas-solid flow direction. So, both of them are positive. This figure also shows that the spatial distributions of the gas-solid drag force and PGF are not uniform. It can be seen that both forces are lower in the stepped section than both sides. The spatial distribution of gas-solid drag force should correspond to the distribution of particle concentration (Figure 14). Where the spatial concentration of particle is high, the gas-solid drag force will be high. The spatial distribution of PGF should correspond to the distribution of static pressure (Figure 4), in which part the static pressure change is more significant, and the PGF should be bigger.

Figure 18 shows the distribution of gas-solid interaction force in X and Y directions. It can be seen that the gas-solid interaction force in X direction is much larger than the force in Y direction. As the stepped pipe is horizontal and X direction is the gas-solid flow direction, this suggests that the gas-solid interaction force in X direction is more important in the horizontal pneumatic conveying system.

4.2.2. Solid-Solid Interaction Force. Solid-solid interaction force relates directly to solid breakage, solid degradation, or attrition. The total and averaged solid-solid interaction force

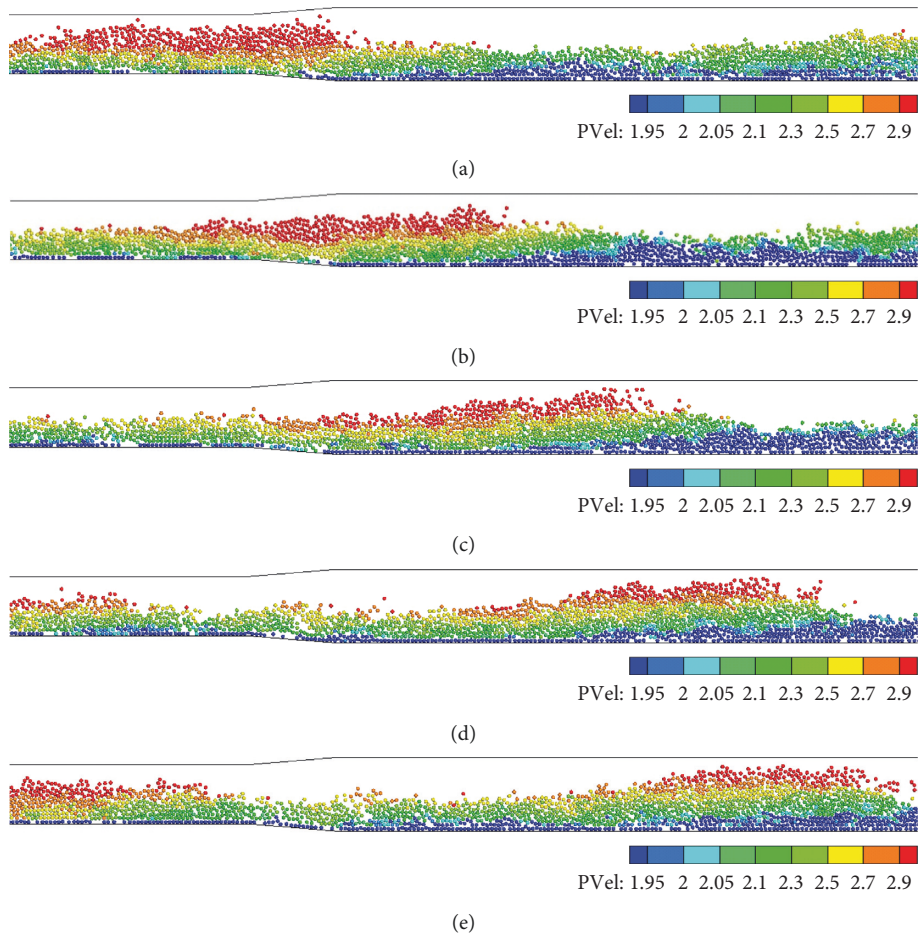

Figure 13: Spatial distribution of solid velocity when a dune passes through the stepped section with CFD-DEM. (a) 3.62 s. (b) 3.65 s. (c) 3.68 s. (d) 3.71 s. (e) 3.74 s.

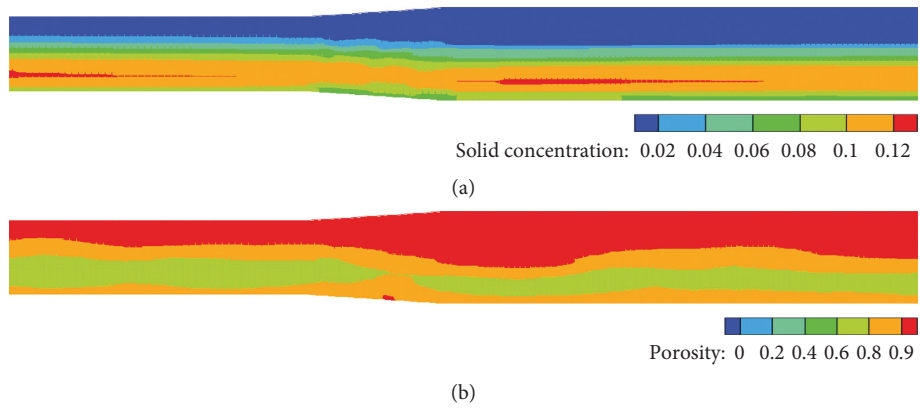

Figure 14: Distribution of time-averaged solids concentration (a) and porosity (b) for the gas-solid flow when a dune passes through the stepped section with CFD-DEM.

can be found in Figure 15. The figure indicates that both the total and averaged solid-solid interaction forces are much larger than the gas-solid drag force, pressure gradient force, and solid-wall interaction fore, suggesting that the inclusion of solid-solid interaction is important in the modelling of gas-solid flows in pneumatic conveying. Further, it can be seen form Figure 15 that the total solid-solid force and averaged force both increases with the solid loading ratio. This is because the solid particles number increases with the solid loading ratio, and the larger the solids number in the pipe, the bigger the chance for solid-solid interactions.

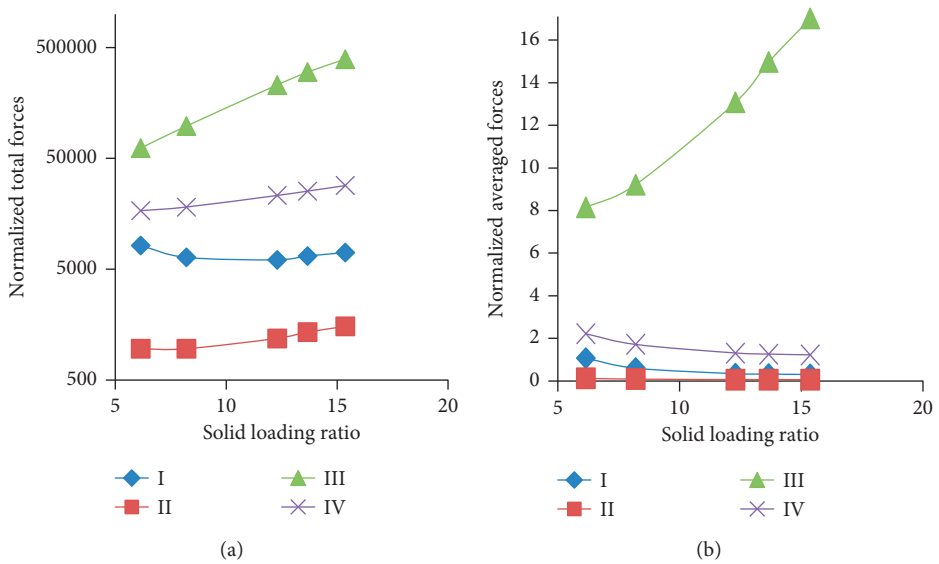

Figure 15: (a) Normalized total force and (b) averaged forces in the stepped pipeline under different solid loading ratios with CFD-DEM: I, gas-solid drag force; II, pressure gradient force; III, solid-solid interaction force; IV, solid-wall interaction force.

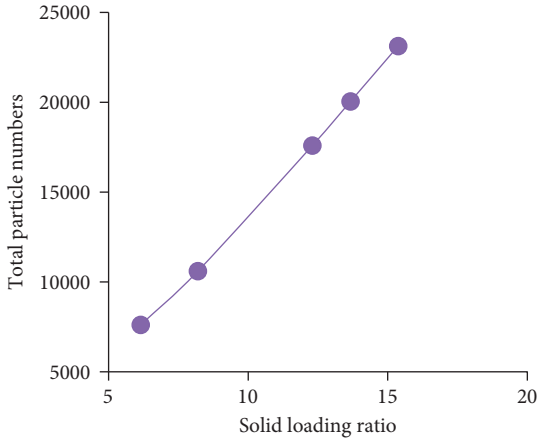

Figure 16: Relationship between the particle number and solid loading ratio with CFD-DEM.

Figure 19 shows the spatial distribution of solid-solid interaction force when a dune passes through the stepped section. It can be seen clearly that the solid-solid force in the stepped section is lower than the forces in both sides, especially the section close to the stepped section in both sides. The high solid-solid interaction force in both sides of the pipeline is due to the solids concentration in these two sections being relatively high, and thus, solids have chance to collide with other solids. The reason for the low solid-solid interaction force in the stepped section can be explained as follows: due to the effect of inertia from the high velocity solids layer which comes from the section before the stepped part and gravity due to the change of pipe geometry, the solid velocity in this part is high (Figure 13) while the porosity here is also high (Figure 14(b)), the solids distribution in this part is more "loose." Thus, the chance of solid collisions with other solids is low. From Figures 19(a)–19(d), it can be seen that the solid-solid interaction force in the section which is just before the stepped part becomes smaller and smaller, while the force in the section just behind the stepped part becomes bigger and bigger. The reason for the force to become smaller and smaller is due to the solids dune in this part passing through the stepped section gradually, with less and less particles leaving there. The particle collisions become weaker gradually. The reason for the force to become larger and larger is mainly due to the hindering function of the thick low-velocity solids layer. During the moving process of the dune, the number of high-velocity particles which collide with the low-velocity solids after the stepped section increases gradually. Therefore, as the solid velocity decreases, more and more particles collide with each other, and a long dune is formed, where the solid-solid interaction force reaches its maximum (Figure 19(d)).

Figure 20 shows the spatial distribution of time-averaged solid-solid interaction force. It can be seen very clearly form this figure that the solid-solid force in the stepped section is the lowest while the section which just behind the stepped part has the largest solid-solid force, and the section before the stepped part also has a relatively higher solid-solid force. Figure 20 further explains the phenomenon observed in Figure 19 and provides a better understanding of the mechanisms governing the gas-solid flow in the stepped section.

4.2.3. Solid-Wall Interaction Force. Solid-wall interaction force is related directly to the wearing of conveying pipe wall which could be a serious problem for a pneumatic conveying system which needs to operate with high gas velocity. Until now, publications on the pipe wearing problem in the stepped pipeline are very limited. This problem will be investigated through the solid-wall interaction force in this section.

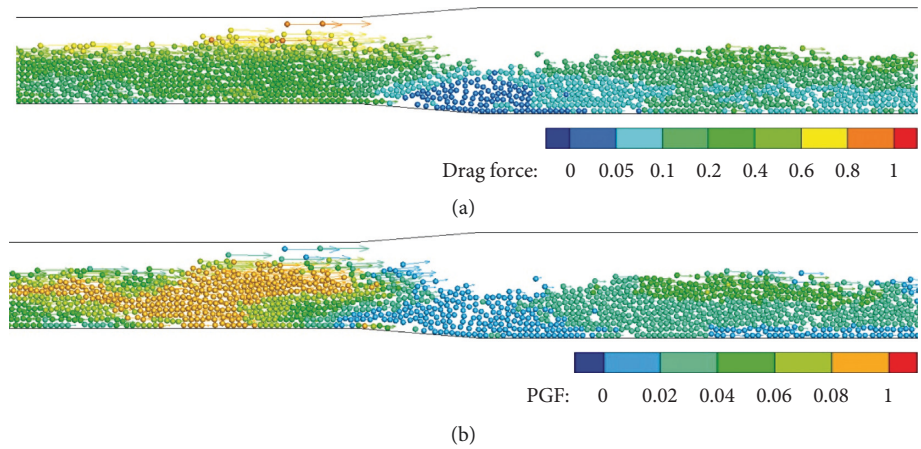

Figure 17: (a) Spatial distribution of gas-solid drag force and (b) PGF near the stepped section with CFD-DEM.

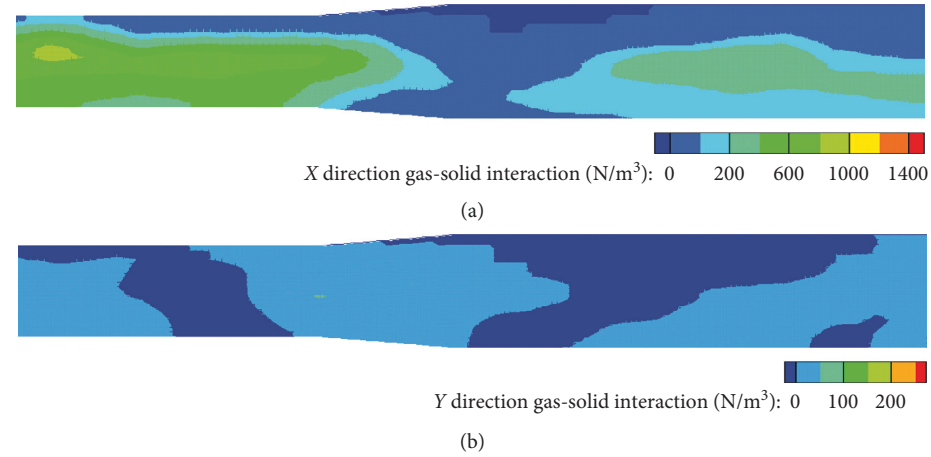

Figure 18: Distribution of gas-solid interaction force in different directions with CFD-DEM: (a) X direction and (b) Y direction.

The total and averaged solid-wall interaction forces are shown in Figure 15. This figure indicates that the value of the total and averaged solid-wall interaction forces are much larger than the gas-solid drag force and pressure gradient force and only slightly lower than the solid-solid interaction force, suggesting that the inclusion of solid-wall interaction force is an important factor in the modelling of gas-solid flows in pneumatic conveying systems. More importantly, Figure 15(a) indicates that the total solid-wall interaction force increasing with the solid loading ratio. This is due to the solids number increasing with the solid loading ratio (Figure 16); the larger the solids number in the pipe, the larger the number of particles that collide with walls. Figure 15(b) shows that the averaged solid-wall force decreases with the solid loading ratio. This may be caused by the "shielding" effect of low solid velocity layer. Not all particles can collide with the wall since some particles only collide with the other particles and bounce back after colliding with the wall [44].

Figure 21 shows the spatial distribution of time-averaged solid-wall interaction force near the stepped section. It can be seen that the particle-wall interaction force is the lowest in the stepped section. The reason for this is similar to the particle-particle interaction force in this section. The solids concentration in this part is very "loose." The solids which can collide with wall are limited. The solid-wall interaction force in the section before the stepped part is relatively large. This is due to the small solid dunes being formed in this part. Large solids concentration (Figure 14(a)) appeared in this section, and the number of solids which collide with wall increase. The largest solid-wall interaction force appears in the section which is just behind the stepped part. Due to the hindering effects of the thick low-velocity solid layer, the solids in the high-velocity solid layer coming from the stepped part collides intensely with the wall and low-velocity solids in this section. Hence, the solid-wall interaction force is larger in this area. A larger solid-wall interaction force means that more serious pipe wall wearing problem happens in this part, and this suggests that a suitable treatment, like increasing the pipe wall thickness in this section, should be done in industrial application based on the simulation works. So, this work not only just helps us understand the mechanisms governing the gas-solid flow in the stepped section better, but also is a good reference for better design, optimization, and scale-up of stepped pipelines.

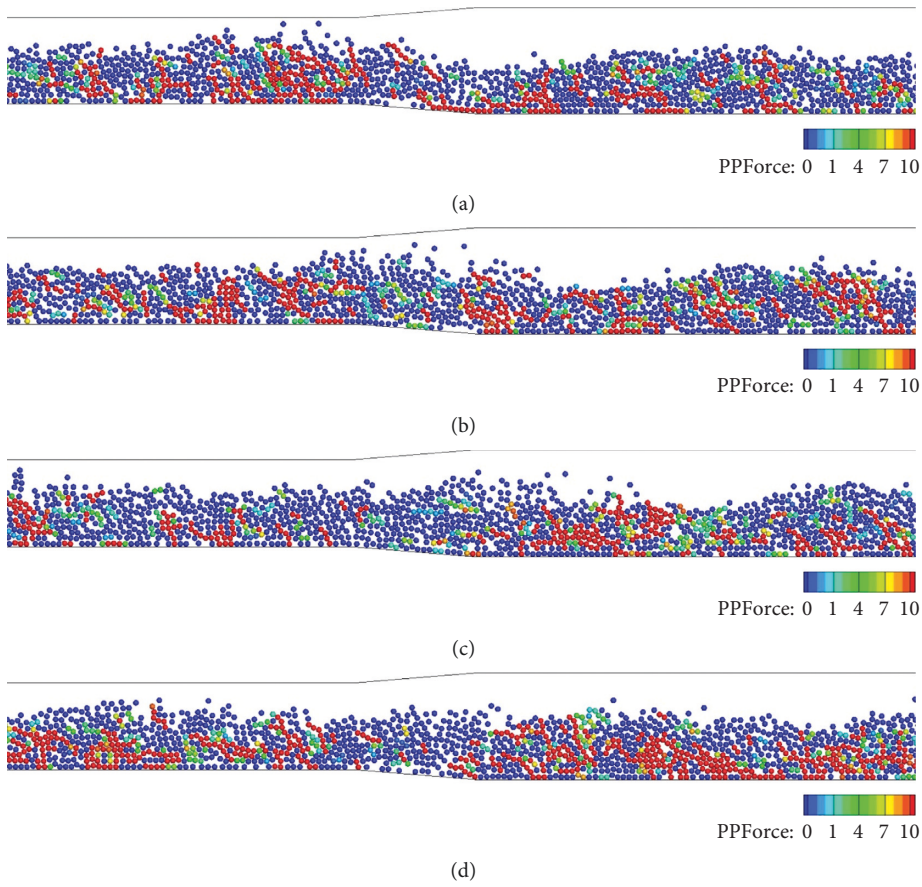

Figure 19: Spatial distribution of solid-solid interaction force when a dune passes through the stepped section with CFD-DEM. (a) 3.86 s. (b) 3.88 s. (c) 3.90 s. (d) 3.92 s.

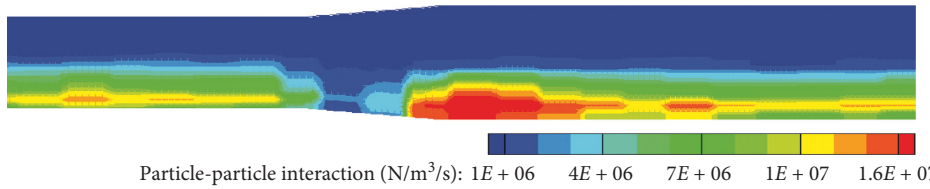

Figure 20: Spatial distribution of time-averaged particle-particle interaction force near the stepped section with CFD-DEM.

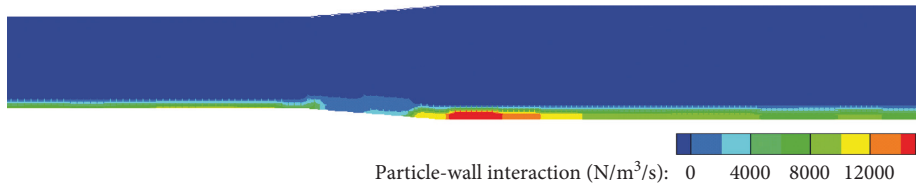

Figure 21: Spatial distribution of time-averaged particle-wall interaction force near the stepped section with CFD-DEM.

5. Conclusions

Both TFM and a CFD-DEM model have been used to study the gas-solid flow in a stepped pipeline. The mechanism governing the gas-solid flow in this system has been revealed through the investigation of pressure drop, gas and solid velocity, and gas-solid flow pattern. Comparison of the computational results with some published experimental work, simulation study, and theoretical analysis results reveals a good agreement. The appearance of large-size solid dunes and pressure surge phenomena suffered in the stepped pipeline have been studied too. The reason of the solid dune is that when the high-velocity solids layer meets with the low-velocity solids layer in the stepped part, a solid superposition phenomenon happens. When the dune moves along the pipe, the high velocity layer in the upper part of the

dune continually picks up a relatively thick low-velocity layer of solids in front of it, the solids dune becomes larger and larger. The appearance of large size solid dune increases the chance of potential blockage and also causes the appearance of pressure surge due to the resistance from solid dune. The section in which the blockage problem most likely occurs in the pipeline is confirmed, the large size solid dunes are mainly formed in the section which is just behind the stepped section, and the blockage problem most likely occurs in this section. The forces governing the motion of gas and solids in the stepped pipeline and the effect of solids loading ratio have also been simulated and investigated. The pipe wearing problem in the stepped pipeline is explored through the distribution of particle-wall interaction force for the first time. The computational results reveal that most serious pipe wall wearing problems happens in the section just behind the stepped part and that suitable treatment should be done for this part in industrial application.

Finally, it should be pointed out that the present study is carried out for large particles. For fine particles, the predictions may be different to some extent. Thus, the present study is largely preliminary, aiming to understand the mechanisms governing the gas-solid flow behaviours in the stepped pipeline, especially in the stepped section, both from microscopic and macroscopic viewpoints. Moreover, publications on stepped pipelines are so limited. The work in this study should be a reference for further design, optimization, and scale-up of stepped pipelines.

Nomenclature

$\mathbf{f}_c$: Contact force (N)
$\mathbf{f}_d$: Damping force (N)
$\mathbf{f}_{pf,i}$: Interparticle forces between particles i and j (N)
F_{pf}: Particle-fluid interaction force (N)
$\mathbf{g}$: Gravity acceleration vector (9.81 m/s^2)
G_i: Gravity vector (N)
I: Moment of inertia of a particle ($kg*$m/s)
k_c: Number of particles in a computational cell
m: Mass of a particle (kg)
$\mathbf{M}$: Rolling friction torque (Nm)
d: Pipeline diameter (mm)
L: Pipeline length (m)
p: Pressure (Pa)
Δp: Pressure drop (Pa)
P: Pressure
t: Time (s)
Δt: Time step for solids (s)
T: Air temperature (°C)
$\mathbf{T}$: Driving friction torque (Nm)
$\mathbf{u}$: Fluid velocity (m/s)
$\dot{V}$: Air flow rate (kg/s)
V_g: Gas velocity (m/s)

Greek Letters

ε: Porosity (dimensionless)
ρ: Density (kg/m^3)
$\boldsymbol{\tau}$: Viscous stress tensor (N/m^3)
$\boldsymbol{\omega}_i$: Rotational velocities of particle i (rad/s).

Data Availability

The Fluent CAS and DAT data used to support the findings of this study are available from the corresponding author upon request.

Conflicts of Interest

The authors declare that they have no conflicts of interest.

Acknowledgments

The authors are grateful to the Australia Research Council (ARC), Fujiang Longking Co., Ltd., Nature Science Foundation of China (51675218 and 51364014), Doctor Starting Foundation of Jiangxi University of Science and Technology of China (JXXJBS17078), Science and Technology Project of the Education Department of Jiangxi Province (GJJ180426), Innovation and Entrepreneurship Project (DC2018-017 and 2018YCTS008), and Jiangsu Provincial Natural Science Foundation (BK20180287).

References

[1] D. Mills, *Pneumatic Conveying Design Guide*, Butterworths, London, UK, 3rd edition, 2016.
[2] D. Mills, *Pneumatic Conveying Design Guide*, Butterworths, London, UK, 2nd edition, 2004.
[3] D. Yang, B. Xing, J. Li, Y. Wang, N. Hu, and S. Jiang, "Experiment and simulation analysis of the suspension behavior of large (5–30 mm) nonspherical particles in vertical pneumatic conveying," *Powder Technology*, vol. 354, pp. 442–455, 2019.
[4] H. Tashiro, Y. Tomita, K. Deguchi, and T. Jotaki, "Sudden expansion of gas–solid two phase flow in a pipe," *Physics of Fluids*, vol. 23, no. 4, pp. 663–666, 1980.
[5] H. Tashiro and Y. Tomita, "Sudden expansion of gas-solid two-phase flow in vertical downward flow," *Bulletin of JSME*, vol. 27, no. 232, pp. 2160–2165, 1984.
[6] H. Tashiro and Y. Tomita, "Sudden expansion of gas-solid two-phase flow in vertical upward flow," *Bulletin of JSME*, vol. 28, no. 245, pp. 2625–2629, 1985.
[7] H. Tashiro and Y. Tomita, "Influence of diameter ratio on a sudden expansion of a circular pipe in gas-solid two-phase flow," *Powder Technology*, vol. 48, no. 3, pp. 227–231, 1986.
[8] J. R. Fesler and J. K. Eaton, "Particle response in a planar sudden expansion flow," *Experimental Thermal and Fluid Science*, vol. 15, no. 4, pp. 413–423, 1997.
[9] A. Goodarz and C. Qian, "Dispersion and deposition of particles in a turbulent pipe flow with sudden expansion," *Journal of Aerosol Science*, vol. 29, no. 9, pp. 1097–1116, 1998.
[10] M. Founti, T. Achimastos, and A. Klipfel, "Effects of increasing particle loading in an axisymmetric, vertical, liquid-solid sudden expansion flow," *Journal of Fluids Engineering*, vol. 121, no. 1, pp. 171–178, 1999.
[11] M. Founti and A. Klipfel, "Experimental and computational investigations of nearly dense two-phase sudden expansion flows," *Experimental Thermal and Fluid Science*, vol. 17, no. 1-2, pp. 27–36, 1998.

[12] L. H. Back and E. J. Roschke, "Shear-layer flow regimes and wave instabilities and reattachment lengths downstream of an abrupt circular channel expansion," *Journal of Applied Mechanics*, vol. 39, no. 3, pp. 677–681, 1972.

[13] P. Monnet, C. Menard, and D. Sigli, "Some new aspects of the slow flow of a viscous fluid through an axisymmetric duct expansion or contraction. II—Experimental part," *Applied Scientific Research*, vol. 39, no. 3, pp. 233–248, 1982.

[14] K. J. Hammad, M. V. Ötügen, and E. B. Arik, "A PIV study of the laminar axisymmetric sudden expansion flow," *Experiments in Fluids*, vol. 26, no. 3, pp. 266–272, 1999.

[15] M. Y. Gundogdu, A. I. Kutlar, and H. Duz, "Analytical prediction of pressure loss through a sudden-expansion in two-phase pneumatic conveying lines," *Advanced Powder Technology*, vol. 20, no. 1, pp. 48–54, 2009.

[16] Y. Bae and Y. I. Kim, "Prediction of local loss coefficient for turbulent flow in axisymmetric sudden expansions with a chamfer: effect of Reynolds number," *Annals of Nuclear Energy*, vol. 73, pp. 33–38, 2014.

[17] Y. Bae and Y. I. Kim, "Prediction of local pressure drop for turbulent flow in axisymmetric sudden expansions with chamfered edge," *Chemical Engineering Research and Design*, vol. 92, no. 2, pp. 229–239, 2014.

[18] H. P. Zhu, Z. Y. Zhou, R. Y. Yang, and A. B. Yu, "Discrete particle simulation of particulate systems: theoretical developments," *Chemical Engineering Science*, vol. 62, no. 13, pp. 3378–3396, 2007.

[19] H. P. Zhu, Z. Y. Zhou, R. Y. Yang, and A. B. Yu, "Discrete particle simulation of particulate systems: a review of major applications and findings," *Chemical Engineering Science*, vol. 63, no. 23, pp. 5728–5770, 2008.

[20] L. Li, H. Qi, Z. C. Yin et al., "Investigation on the multiphase sink vortex Ekman pumping effects by CFD-DEM coupling method," *Powder Technology*, 2019, In press.

[21] S. B. Kuang, M. M. Zhou, and A. B. Yu, "CFD-DEM modelling and simulation of pneumatic conveying: a review," *Powder Technology*, 2019, In press.

[22] J. Heng, T. H. New, and P. A. Wilson, "Application of an Eulerian granular numerical model to an industrial scale pneumatic conveying pipeline," *Advanced Powder Technology*, vol. 30, no. 2, pp. 240–256, 2019.

[23] H. Qi, D. Wen, Q. Yuan, L. Zhang, and Z. Chen, "Numerical investigation on particle impact erosion in ultrasonic-assisted abrasive slurry jet micro-machining of glasses," *Powder Technology*, vol. 314, pp. 627–634, 2017.

[24] T. B. Anderson and R. Jackson, "Fluid mechanical description of fluidized beds. Equations of motion," *Industrial & Engineering Chemistry Fundamentals*, vol. 6, no. 4, pp. 527–539, 1967.

[25] D. Gidaspow, *Multiphase Flow and Fluidization*, Academic Press, San Diego, CA, USA, 1994.

[26] H. Enwald, E. Peirano, and A. E. Almstedt, "Eulerian two-phase flow theory applied to fluidization," *International Journal of Multiphase Flow*, vol. 22, pp. 21–66, 1996.

[27] Y. Q. Feng and A. B. Yu, "Assessment of model formulations in the discrete particle simulation of Gas–Solid flow," *Industrial & Engineering Chemistry Research*, vol. 43, no. 26, pp. 8378–8390, 2004.

[28] Z. Miao, S. Kuang, H. Zughbi, and A. Yu, "CFD simulation of dilute-phase pneumatic conveying of powders," *Powder Technology*, vol. 349, pp. 70–83, 2019.

[29] Y. Tsuji, T. Tanaka, and T. Ishida, "Lagrangian numerical simulation of plug flow of cohesionless particles in a horizontal pipe," *Powder Technology*, vol. 71, no. 3, pp. 239–250, 1992.

[30] Y. Tsuji, T. Kawaguchi, and T. Tanaka, "Discrete particle simulation of two-dimensional fluidized bed," *Powder Technology*, vol. 77, no. 1, pp. 79–87, 1993.

[31] B. H. Xu and A. B. Yu, "Numerical simulation of the gas-solid flow in a fluidized bed by combining discrete particle method with computational fluid dynamics," *Chemical Engineering Science*, vol. 52, no. 16, pp. 2785–2809, 1997.

[32] Z. Y. Zhou, S. B. Kuang, K. W. Chu, and A. B. Yu, "Discrete particle simulation of particle-fluid flow: model formulations and their applicability," *Journal of Fluid Mechanics*, vol. 661, pp. 482–510, 2010.

[33] K. W. Chu and A. B. Yu, "Numerical simulation of the Gas–Solid flow in three-dimensional pneumatic conveying bends," *Industrial & Engineering Chemistry Research*, vol. 47, no. 18, pp. 7058–7071, 2008.

[34] H. Zhao and Y. Zhao, "CFD-DEM simulation of pneumatic conveying in a horizontal channel," *International Journal of Multiphase Flow*, vol. 118, pp. 64–74, 2019.

[35] K. W. Chu and A. B. Yu, "Numerical simulation of complex particle-fluid flows," *Powder Technology*, vol. 179, no. 3, pp. 104–114, 2008.

[36] P. A. Cundall and O. D. L. Strack, "A discrete numerical model for granular assemblies," *Géotechnique*, vol. 29, no. 1, pp. 47–65, 1979.

[37] K. W. Chu and A. B. Yu, "Numerical and experimental investigation of an "S-shaped" circulating fluidized bed," *Powder Technology*, vol. 254, pp. 460–469, 2014.

[38] H. Wahyudi, K. Chu, and A. Yu, "3D particle-scale modeling of gas-solids flow and heat transfer in fluidized beds with an immersed tube," *International Journal of Heat and Mass Transfer*, vol. 97, pp. 521–537, 2016.

[39] K. W. Chu, B. Wang, A. B. Yu, and A. Vince, "Computational study of the multiphase flow in a dense medium cyclone: effect of particle density," *Chemical Engineering Science*, vol. 73, pp. 123–139, 2012.

[40] K. Chu, J. Chen, and A. Yu, "Applicability of a coarse-grained CFD-DEM model on dense medium cyclone," *Minerals Engineering*, vol. 90, pp. 43–54, 2016.

[41] D. Mills and J. S. Mason, "An analysis of stepped pipelines for pneumatic conveying systems," in *Proceedings of the 12th Powder and Bulk Solids Conference*, pp. 696–704, Chicago, IL, USA, May 1987.

[42] P. W. Wypych and J. Yi, "Minimum transport boundary for horizontal dense-phase pneumatic conveying of granular materials," *Powder Technology*, vol. 129, no. 1–3, pp. 111–121, 2003.

[43] S. B. Kuang and A. B. Yu, "Micromechanic modeling and analysis of the flow regimes in horizontal pneumatic conveying," *AIChE Journal*, vol. 57, no. 10, pp. 2708–2725, 2011.

[44] K. W. Chu, B. Wang, D. L. Xu, Y. X. Chen, and A. B. Yu, "CFD-DEM simulation of the gas-solid flow in a cyclone separator," *Chemical Engineering Science*, vol. 66, no. 5, pp. 834–847, 2011.